Simulation assessment of the direct-push permeameter for characterizing vertical variations in hydraulic conductivity

Gaisheng Liu,[1] Geoffrey C. Bohling,[1] and James J. Butler Jr.[1]

Received 31 March 2007; revised 5 September 2007; accepted 8 October 2007; published 22 February 2008.

[1] The direct-push permeameter (DPP) is a tool for the in situ characterization of hydraulic conductivity (K) in shallow, unconsolidated formations. This device, which consists of a short screened section with a pair of pressure transducers near the screen, is advanced into the subsurface with direct-push technology. K is determined through a series of injection tests conducted between advancements. Recent field work by Butler et al. (2007) has shown that the DPP holds great potential for describing vertical variations in K at an unprecedented level of detail, accuracy and speed. In this paper, the fundamental efficacy of the DPP is evaluated through a series of numerical simulations. These simulations demonstrate that the DPP can provide accurate K information under conditions commonly faced in the field. A single DPP test provides an effective K for the domain immediately surrounding the interval between the injection screen and the most distant pressure transducer. Features that are thinner than that interval can be quantified by reducing the vertical distance between successive tests and analyzing the data from all tests simultaneously. A particular advantage of the DPP is that, unlike most other single borehole techniques, a low-K skin or a clogged screen has a minimal impact on the K estimate. In addition, the requirement that only steady-shape conditions be attained allows for a dramatic reduction in the time required for each injection test.

Citation: Liu, G., G. C. Bohling, and J. J. Butler Jr. (2008), Simulation assessment of the direct-push permeameter for characterizing vertical variations in hydraulic conductivity, *Water Resour. Res.*, *44*, W02432, doi:10.1029/2007WR006078.

1. Introduction

[2] Variations in hydraulic conductivity (K) over very short distances can clearly play an important, if not dominant, role in subsurface solute transport processes [*Boggs et al.*, 1993; *Feehley et al.*, 2000; *Harvey and Gorelick*, 2000; *Liu et al.*, 2004; *Berkowitz et al.*, 2006]. Contrary to assumptions made in early transport studies, these small-scale heterogeneities may not be simply averaged out (i.e., homogenized), as the concentration evolution of solutes in groundwater can be extremely sensitive to the details of such variations. Despite the widespread recognition of the importance of small-scale geological control, we still lack effective tools for characterization of K at the resolution required for transport studies [*Butler*, 2005].

[3] The direct-push permeameter (DPP) is a promising tool for the high-resolution characterization of vertical variations in K. The DPP is a small-diameter tool with a short screened section and a pair of pressure transducers near the screen (Figure 1). The tool is advanced into the shallow subsurface with direct-push technology. At depth intervals where a K estimate is desired, advancement ceases and a series of injection tests are conducted. Although the DPP was first introduced by *Stienstra and van Deen* [1994] in the Netherlands and later developed by *Lowry et al.* [1999] in the United States, the tool is still in the prototype stage. Recently, however, *Butler et al.* [2007] demonstrated that the DPP holds great potential for obtaining high-resolution K information quickly and accurately. Motivated by these findings, we investigate here the fundamental efficacy of the DPP through numerical simulation.

[4] Several direct-push techniques for estimating K are currently available [*Hinsby et al.*, 1992; *Lunne et al.*, 1997; *Butler et al.*, 2002; *Dietrich and Leven*, 2005; *McCall et al.*, 2005; *Sellwood et al.*, 2005]. The zone of compaction that can be created in the immediate vicinity of a direct-push borehole during tool advancement has adversely affected the performance of most of these techniques [*Butler et al.*, 2002]. Other major limitations of these techniques include screen clogging during tool advancement, and, for slug testing, the length of time required for development of each test interval [*Butler et al.*, 2002; *McCall et al.*, 2002; *Sellwood et al.*, 2005]. However, as discussed in *Butler et al.* [2007], the DPP appears to be largely unaffected by these limitations.

[5] Despite its considerable potential, the DPP has not been utilized beyond a few demonstration projects [*Lowry et al.*, 1999; *Butler et al.*, 2007]. Moreover, other than one initial study [*Lowry et al.*, 1999], a simulation assessment has not been performed to evaluate the validity of the DPP systematically. Thus there are still many questions about the performance of the tool under common field conditions.

[6] In this study, the DPP is investigated using a high-resolution numerical model. A series of DPP tests are simulated at different positions within an hypothetical aquifer that is based on conditions at the Geohydrologic Experimental and Monitoring Site (GEMS), a site at which

[1]Kansas Geological Survey, University of Kansas, Lawrence, Kansas, USA.

0043-1397/08/2007WR006078

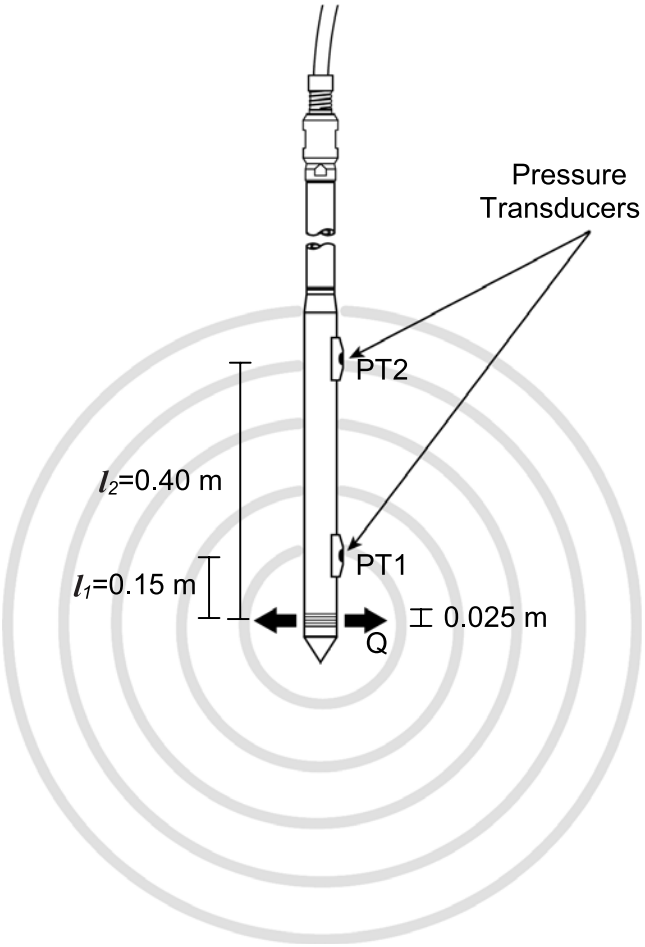

Figure 1. Schematic of the DPP evaluated in this work [after *Butler et al.*, 2007]. The gray thick circles are a qualitative illustration of the equipotential lines under the assumption of point injection in a homogeneous and isotropic aquifer (figure not to scale).

a great deal of previous work has been done [*Butler*, 2005; *Butler et al.*, 2007; *Bohling et al.*, 2007]. The impact of different factors, including a low-K skin, screen clogging, anisotropy, and small-scale barriers and pathways for flow, are investigated. The difference in the time required to attain steady-shape versus steady state conditions is also explored. The code *lr2dinv* [*Bohling and Butler*, 2001], which has been developed for the simulation and analysis of hydraulic tests in cylindrical flow systems, is used to simulate the DPP tests and invert the K values from the simulated DPP responses. The inverted K estimates are then compared to the input reference K values to assess how the DPP performs in each simulation. Adjoint sensitivity analyses are conducted to provide further insights into the performance of the DPP under various hydrogeological settings.

[7] The remainder of this paper proceeds as follows. We start by providing a brief description of the DPP. Two simple analytical formulas are presented for calculating K assuming ideal point injection in a homogeneous, spherically infinite medium. We then describe the development of the numerical model with which the DPP is evaluated, after which, we report the simulation results for the various conditions explored here. Finally, we offer some concluding remarks concerning the major findings of this work.

2. The Direct-Push Permeameter

[8] The DPP consists of two major components: a short screened section through which water is injected into the formation and a pair of pressure transducers (PT1 and PT2) that measure the head changes induced by that injection (Figure 1). The DPP is attached to the end of a string of steel pipe and advanced into the subsurface with direct-push equipment. During pushing, water is injected continuously to prevent screen clogging. When the desired depth for a K measurement is reached, pushing and water injection cease and the heads in the aquifer are allowed to recover to background levels. A short hydraulic test is then conducted at a given injection rate, Q, while head changes are monitored at the two transducers. A K estimate can be obtained from the head changes using an equation based on the spherical form of Darcy's Law [*Lowry et al.*, 1999; *Butler et al.*, 2007],

$$K = \frac{Q}{4\pi(\Delta h_1 - \Delta h_2)}\left(\frac{1}{l_1} - \frac{1}{l_2}\right), \tag{1}$$

where l_1 and l_2 are the distances from the center of the screen to the near (PT1) and far (PT2) transducers, respectively (Figure 1); and Δh_1 and Δh_2 are the head changes from the background levels at PT1 and PT2, respectively. The head changes are typically recorded over a period of time to average out sensor noise and small-scale variations in flow rate. The derivation of (1) assumes a point injection in a homogenous, isotropic, spherically infinite medium. If the medium is anisotropic and the principal axes of anisotropy are in the vertical and horizontal planes, equation (1) will provide an estimate of the horizontal component of K [*Butler et al.*, 2007]. An alternative approach for estimating K is to use the head change (Δh_i) at individual transducers at steady state [*Butler et al.*, 2007],

$$K_i = \frac{Q}{4\pi l_i(\Delta h_i)}, \qquad i = 1 \text{ or } 2. \tag{2}$$

[9] An important advantage of equation (1) is that only steady-shape conditions are required (i.e., the difference $\Delta h_1 - \Delta h_2$ does not change with time), which can occur long before steady-state conditions (i.e., the individual head changes, Δh_1 and Δh_2, do not change with time) required for equation (2) are attained [*Butler*, 1990; *Bohling et al.*, 2002]. Thus equation (1) is typically used in the preliminary data analysis. When the medium is highly heterogeneous, equation (2) can be used to help identify the existence of a thin layer of extreme properties between the two transducers [*Butler et al.*, 2007].

3. Model Development

3.1. Governing Equations

[10] Flow under the DPP test conditions can be readily described using a cylindrical coordinate system. Assuming a confined flow system and symmetry in the angular direction, the governing equation for the movement of ground-

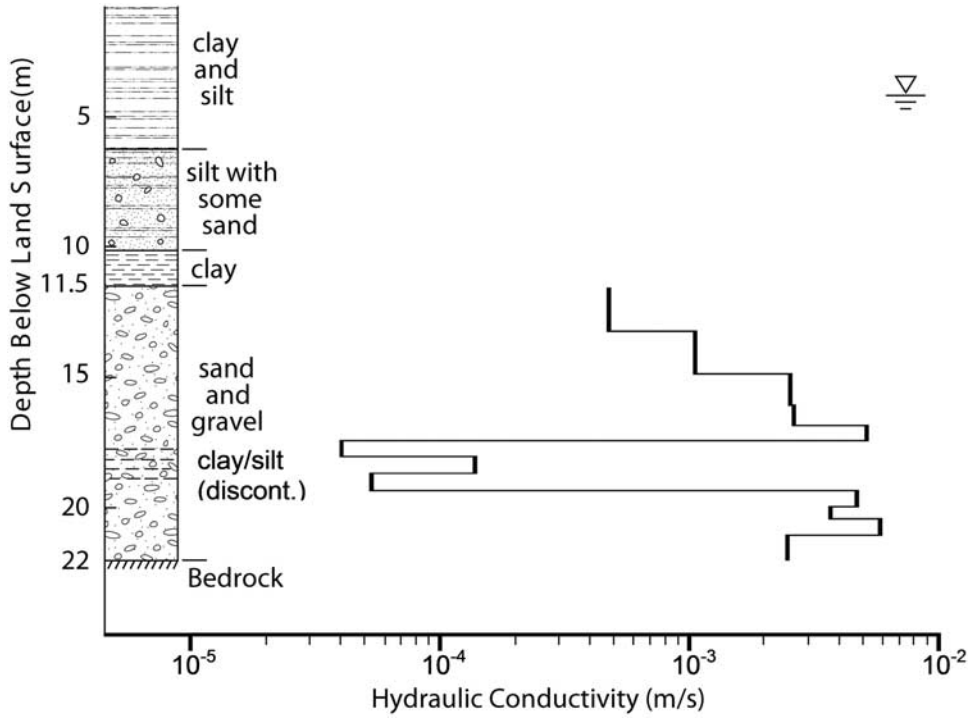

Figure 2. Shallow stratigraphy at the GEMS research site and the K profile measured in the DPP field assessment of *Butler et al.* [2007]. The low-K clay and silt layer in the sand and gravel interval is discontinuous.

water can be written as,

$$\frac{1}{r}\frac{\partial}{\partial r}\left(rK_r\frac{\partial h}{\partial r}\right)+\frac{\partial}{\partial z}\left(K_z\frac{\partial h}{\partial z}\right)=S_S\frac{\partial h}{\partial t}, \tag{3}$$

where the head h is a function of the radial coordinate r, vertical coordinate z, and time t; K_r is the radial hydraulic conductivity; K_z is the vertical hydraulic conductivity; and S_S is the specific storage. By introducing a logarithmic transformation of the radial coordinate, $r' = ln\ (r/r_w)$, equation (3) can be converted into an equivalent Cartesian flow equation [*Butler and McElwee*, 1995],

$$\frac{\partial}{\partial r'}\left(K_r\frac{\partial h}{\partial r'}\right)+\frac{\partial}{\partial z}\left(K'_z\frac{\partial h}{\partial z}\right)=S'_S\frac{\partial h}{\partial t}, \tag{4}$$

where $K'_z = r^2K_z = r^2\gamma K_r$; and $S'_S = r^2S_S$; γ is the vertical to horizontal anisotropy ratio K_z/K_r.

[11] At the inner boundary $r = r_w$, where r_w is the radius of the DPP tool (0.0225 m in this work), the boundary condition is zero flow except across the injection screen interval b,

$$\left(rK_r\frac{\partial h}{\partial r}\right)_{r=r_w}=\frac{Q}{2\pi b}. \tag{5a}$$

At the outer boundary $r = r_o$, where r_o is the distance from the center of the DPP to the outer edge of the model domain,

$$h|_{r=r_o}=h_0, \tag{5b}$$

where h_0 remains constant through time. The distance to the outer boundary, r_o, is set to a large value so that the boundary has no impact on the simulations reported here. Prior to the start of each DPP injection test, an equilibration period is used to allow the heads to recover to background levels. As a result, the initial heads are set to h_0 in all the simulations.

3.2. Numerical Model

[12] To investigate the DPP in a theoretically rigorous manner, equation (4) is numerically solved with the appropriate initial and boundary conditions using the code *lr2dinv* [*Bohling and Butler*, 2001]. A K profile measured at GEMS is used as the reference K field for the model (Figure 2). The shallow subsurface at that site consists of ~10.7 m of highly conductive alluvial sand and gravel deposits that are overlain and hydraulically confined by ~11.5 m of silt and clay, and underlain by low-K bedrock [*Schulmeister et al.*, 2003; *Butler*, 2005]. On the basis of large-scale pumping tests at the site, the depth-averaged K_r of the entire aquifer is estimated to be 1.5×10^{-3} m/s [*Bohling and Butler*, 2001]. Figure 2 shows a detailed K profile obtained from a DPP field assessment at the site [*Butler et al.*, 2007].

[13] To ensure high numerical accuracy, a fine finite difference grid of 420 layers and 100 cylindrical columns is used to represent the GEMS aquifer. The thickness of each layer, Δz, is constant at 0.025 m, resulting in a simulated aquifer thickness of 10.5 m (depth 11.5 m to 22.0 m on Figure 2). The radial distance between the center of the DPP and that of each cylindrical column j follows an exponential function,

$$r_j = r_w e^{(j-0.5)\Delta r'}, \tag{6}$$

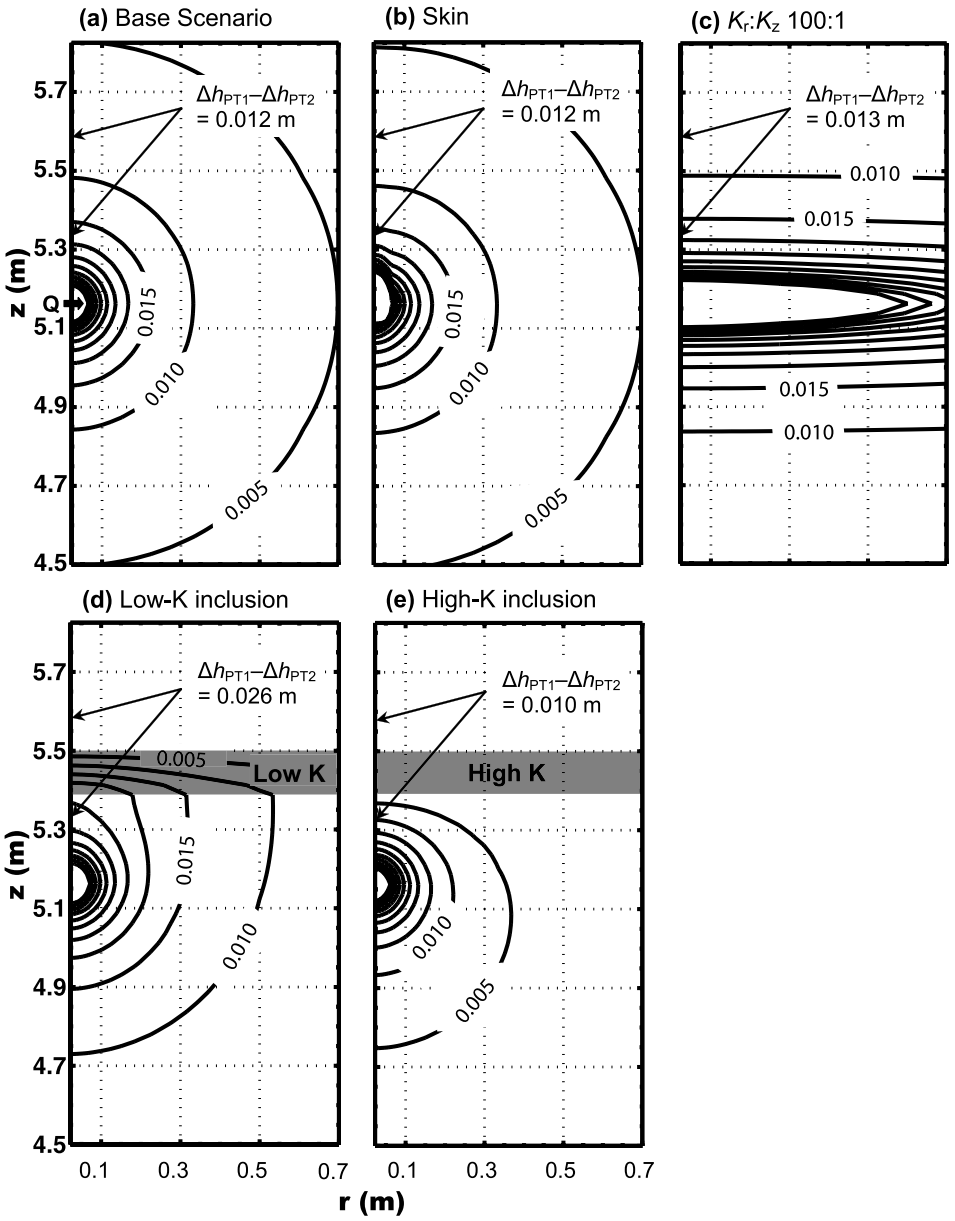

Figure 3. Contours of steady-state head changes induced by a single DPP injection test under different scenarios. The head field for the screen clogging scenario is essentially identical to that in the base scenario and is not plotted.

where the log-transformed radial increment, $\Delta r'$, is set to 0.2. The telescoping dimensions in the radial direction are necessary for the effective representation of DPP test conditions. The distance between the center of the DPP and the outer model boundary is 1.09×10^7 m.

[14] The numerical simulations for each scenario are performed in two phases: 1) Forward Simulation - we apply *lr2dinv* in the forward mode to simulate head changes at the locations corresponding to the two transducers PT1 and PT2 for DPP tests at different depths in the GEMS profile. 2) Inverse Parameter Estimation - we apply *lr2dinv* in the inverse mode to estimate K using the simulated head changes at PT1 and PT2. The inverted K estimates are then compared to the input reference K values to evaluate DPP performance under different hydrogeological settings. K estimates are also calculated using the analytical formula given in equation (1).

3.2.1. Forward Simulation

[15] Forward simulation is used to compute the injection-induced head changes at the transducer locations. Unlike an actual field application where the K distribution is largely unknown, the K field is known during the forward simulation so these input K values, which are based on the K profile measured at GEMS, can be used to assess the accuracy of K estimates determined from the simulated tests. The initial head is set to a constant value (h_0) in all cells and the injection rate Q is maintained constant at 6.0×10^{-5} m^3/s for all scenarios.

Table 1. Results of the Single-Injection, Homogeneous Aquifer Case[a]

		Δh_1 (m)	Δh_2 (m)	K^c (m/s)	K^d (m/s)
Base		0.0201	0.0081	1.65×10^{-3}	1.50×10^{-3}
Clogging		0.0201	0.0081	1.66×10^{-3}	1.51×10^{-3}
Skin[b]		0.0194	0.0077	1.71×10^{-3}	1.55×10^{-3}
Anisotropy of K	1:2	0.0206	0.0081	1.59×10^{-3}	1.45×10^{-3}
(K_z: K_r)	1:10	0.0212	0.0082	1.53×10^{-3}	1.39×10^{-3}
	1:100	0.0214	0.0082	1.50×10^{-3}	1.36×10^{-3}
	1:1000	0.0214	0.0082	1.50×10^{-3}	1.36×10^{-3}

[a]The input reference K_r is 1.50×10^{-3} m/s in all scenarios.
[b]The results are shown for a skin of thickness 0.04 m and K 1.5×10^{-4} m/s.
[c]Calculated based on the analytical formula (1).
[d]Numerically inverted by *lr2dinv*.

3.2.2. Inverse Parameter Estimation

[16] Most of the inputs for the inverse analysis are identical to those used in the forward simulation except that the K is now specified as an unknown parameter for estimation. The simulated head changes at PT1 and PT2 are used as the observed data during the parameter estimation process. In *lr2dinv*, the Levenberg-Marquardt algorithm [*Press et al.*, 1992] is implemented for inverse parameter estimation. This algorithm minimizes the chi-square error measure as given by,

$$\chi^2 = \sum_m \left(\frac{d_m - f_m(K)}{\sigma_m} \right)^2, \tag{7}$$

where d_m represents the simulated difference in the head changes between the two transducers ($\Delta h_1 - \Delta h_2$) from the forward simulation and f_m (K) represents the corresponding difference using the current estimated K values. The scaling factor, σ_m, is often set to the estimated standard deviation associated with the m^{th} observation; however, in this study we have used unweighted regression, setting all the σ_m values to 1, since the simulated DPP data are noise-free. The forward and inverse simulations are performed with the same numerical model, so there is no need to account for any potential errors associated with the model predictions f_m (K). During the parameter estimation process, K values are updated iteratively until the chi-square error or the relative change between successive iterations is less than a user-defined criterion or the total number of iterations exceeds a user-specified limit. To avoid the inverse problem being underdetermined, the number of unknown K values to be estimated is always set equal to or smaller than the number of injection tests.

4. Results and Discussions

[17] Using the model developed in Section 3, we investigate DPP performance under various hydrogeological scenarios. In the following sections, results are presented for cases of increasing complexity.

4.1. Single Injection Test in a Homogeneous Aquifer

[18] This case is designed to provide a straightforward evaluation of the DPP under the simplest conditions. A single injection test is performed with the injection screen placed near the center of the aquifer (5.150 to 5.175 m above the aquifer bottom). The transducers PT1 and PT2 are located 0.15 m and 0.40 m above the screen center, respectively. The input K field is homogeneous and isotropic, with a value set to the depth-averaged K_r of 1.5×10^{-3} m/s. Figure 3(a) shows the contours of injection-induced head changes at steady state for the base scenario. The head changes quickly dissipate with distance from the injection screen. A close examination reveals that, despite an apparent symmetry, the head gradient in the horizontal direction is slightly greater than that in the vertical direction. This is mainly a result of the injection screen being a cylinder. The flow is thus not spherically symmetric in the immediate vicinity of the screen.

[19] Variations are made relative to the base scenario to investigate the importance of screen clogging, a low K skin, and anisotropy. Table 1 summarizes the results of the base scenario and variations of it. In the base scenario, the K estimate calculated with the simple analytical formula (1) is ~10% larger than the input reference value due to the deviations of test conditions from the assumptions embodied in (1). There are two major differences between the flow during a DPP test and that assumed in (1). First, as discussed above, instead of an ideal point, the injection screen is a cylinder. Second, the actual aquifer domain for the DPP tests is not the assumed infinite domain, particularly in the vertical direction. Because of these conceptual differences, numerical analysis is necessary to obtain more accurate K estimates. Nonetheless, equation (1) provides a good initial estimate that can be used for facilitating the convergence of the numerical inversion. *Lowry et al.* [1999] reported a similar discrepancy between the K value calculated using (1) and the actual input K, and noted that this discrepancy should decrease with increasing distance between the transducers and the injection screen.

[20] In the clogging scenario, a thin zone of low-K material is applied over the entire DPP injection screen. The clogged zone is 0.005 m in thickness with a low K value 1.5×10^{-6} m/s. During the numerical inversion, the clogged zone is not explicitly specified and the estimated K field is assumed to be homogeneous. Table 1 displays the results of the clogging simulation. The head changes at both transducers and the resulting K estimates remain similar to those in the base scenario. This indicates that screen clogging during tool advancement has a negligible effect on DPP performance. The only significant impact of screen clogging is that the injection pressure behind the screen is much higher than that when clogging is not present.

[21] In the skin scenario, a low-K zone, represented by a cylindrical column of nodes, is placed around the DPP tool. To mimic the anticipated field conditions, the low-K zone extends from the aquifer top to just below the injection screen. The thickness of the skin zone varies from 0.005 to

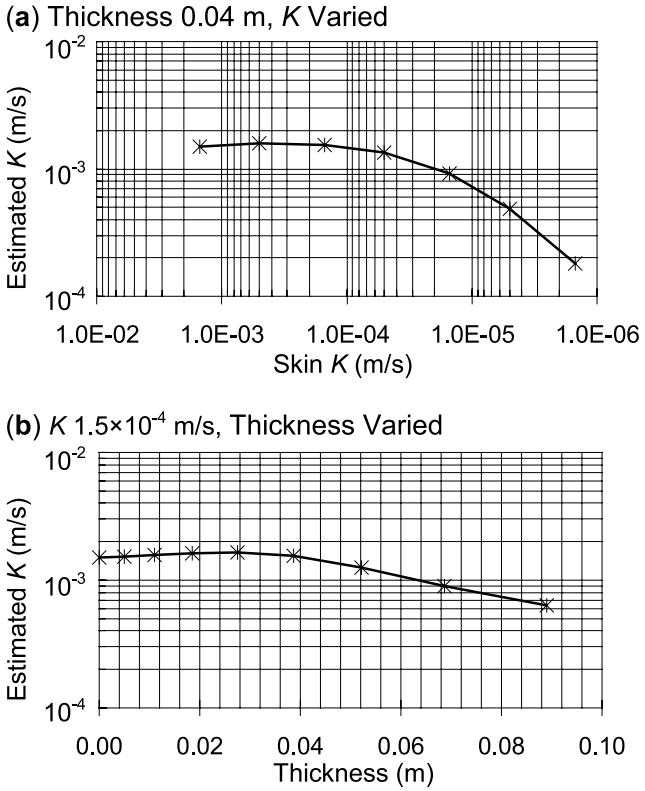

Figure 4. The DPP estimated K values for different skin configurations: (a) Thickness 0.04 m, K varied and (b) K 1.5×10^{-4} m/s, thickness varied.

0.09 m between simulations, and the skin K varies from 1.5×10^{-3} to 1.5×10^{-6} m/s. Other settings remain identical to those in the base scenario. Figure 3(b) shows the induced head changes at steady state for a skin thickness of 0.04 m with a K of 1.5×10^{-4} m/s. Clearly, the presence of the skin has altered the flow field in the immediate vicinity of the screen. However, these effects quickly diminish with distance from the screen, so the difference in the head changes between the two transducers remains close to that in the base scenario (0.012 m).

[22] During the numerical inversion, the skin is not explicitly specified and the aquifer is assumed homogeneous. Table 1 shows the results for a skin with thickness of 0.04 m and a K of 1.5×10^{-4} m/s. The K estimate from the numerical inversion deviates from the input reference value by less than 10%. Figures 4(a) and 4(b) display numerical K estimates for skins of different K values and thicknesses. When the skin K is smaller than $\sim 2.0 \times 10^{-5}$ m/s for a skin thickness of 0.04 m, or the skin thickness is greater than $\sim$0.06 m for a K of 1.5×10^{-4} m/s, the DPP K estimate becomes smaller than 1.0×10^{-3} m/s (a deviation of 33% from the reference value). In many situations, however, the low-K skin formed by advancement of a direct-push tool is expected to be within one order of magnitude of the aquifer K [e.g., *Butler et al.*, 2002].

[23] The impact of anisotropy is investigated by varying the K_z: K_r ratio from 1:2 to 1:1000, while K_r is maintained constant at 1.5×10^{-3} m/s and other conditions are identical to those in the base scenario. Figure 3(c) depicts the induced head changes at an anisotropy ratio of 1:100. Flow is overwhelmingly horizontal because of the anisotropy. The altered flow field does not greatly affect the difference in the head changes between the two transducers, which increases less than 10% relative to that in the base scenario.

[24] Different K estimates for the anisotropic configurations are provided in Table 1. Despite the wide range of anisotropy factors, all the equation (1)-calculated K estimates remain close to the reference K_r value, consistent with results reported in *Butler et al.* [2007]. In the highly anisotropic case, the impact of the point injection assumption in (1) becomes minimal so that there is essentially no difference between the calculated and reference K_r values. The numerically inverted K estimates are obtained by assuming that the K field is isotropic and no information on anisotropy is available. The numerical *lr2dinv* estimates, which are a function of both the vertical and horizontal K, are smaller than the reference K_r value. After the anisotropy factor decreases below 1:100, both the equation (1)-calculated and *lr2dinv*-inverted K estimates show no further significant changes.

[25] To further explore how the DPP is influenced by the K field in a single injection test, we compute the sensitivity of the difference in head changes between the two transducers with respect to K,

$$J_i = \frac{\partial(\Delta h_2 - \Delta h_1)}{\partial K_i / \hat{K}_i}, \tag{8}$$

where ∂K_i is a small perturbation around the base value $\hat{K}_i$ at location i; ∂ $(\Delta h_2 - \Delta h_1)$ is the change in the difference $(\Delta h_2 - \Delta h_1)$ caused by ∂K_i. Here the K field is isotropic so that $K = K_r = K_z$. Scaling the sensitivity by the corresponding parameter value $\hat{K}_i$ gives results that are more indicative of the actual influence of K and allows us to compare more appropriately the values computed at different locations in a heterogeneous setting. Note that the difference $\Delta h_2 - \Delta h_1$ is used instead of $\Delta h_1 - \Delta h_2$ in (8), because $\Delta h_2 - \Delta h_1$ is positively related to the K estimate (see equation (1)). Therefore if the sensitivity of $\Delta h_2 - \Delta h_1$ to the K at location i is a positive value, the DPP K estimate will increase when the K increases at location i, and vice versa.

[26] In this work J_i is computed using the adjoint state method [*Sykes et al.*, 1985; *Sun*, 1994]. The adjoint function, φ, of the head difference $(\Delta h_2 - \Delta h_1)$ under steady-shape conditions is obtained by solving,

$$\frac{\partial}{\partial r'}\left(K_r \frac{\partial \varphi}{\partial r'}\right) + \frac{\partial}{\partial z}\left(K_z' \frac{\partial \varphi}{\partial z}\right) = \delta(r' - r_2')\delta(z - z_2) - \delta(r' - r_1')\delta(z - z_1), \tag{9}$$

where δ is the Dirac delta function; r_1' and r_2' are the log-transformed radial coordinates for PT1 and PT2. Equation (9) is similar to the equation for h itself (i.e., equation (4)), except with a right-hand side forcing function representing the locations of transducers PT2 and PT1. That is, the adjoint function essentially represents an influence function associated with the observed head difference $(\Delta h_2 - \Delta h_1)$. The boundary conditions for the adjoint equation have the same form as those for the flow equation, with all specified-head

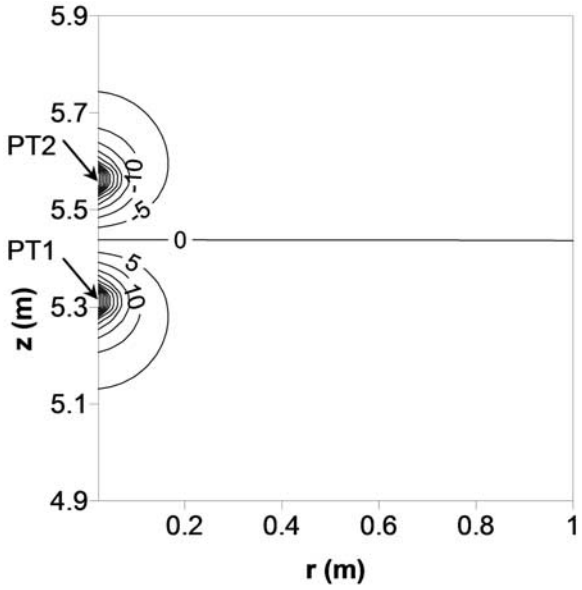

Figure 5. The adjoint function φ of Δh for the base scenario with a homogeneous K of 1.5×10^{-3} m/s.

boundaries being replaced with $\varphi = 0$ and all specified-flux boundaries with $\frac{\partial \varphi}{\partial r'} = 0$ or $\frac{\partial \varphi}{\partial z} = 0$. The normalized sensitivity to the K at location i is then given by,

$$J_i = \hat{K}_i \left[\frac{\partial h}{\partial r'} \frac{\partial \varphi}{\partial r'} + \gamma r^2 \frac{\partial h}{\partial z} \frac{\partial \varphi}{\partial z} \right]_i . \quad (10)$$

[27] Figure 5 shows the adjoint function φ for the base scenario (K of 1.5×10^{-3} m/s). The φ is a dipole field with the positive pole located at the near transducer and the negative pole at the far transducer. Similar dipole fields, although differing in detail, are obtained for all other scenarios described here. Figure 6 depicts the sensitivity of $(\Delta h_2 - \Delta h_1)$ to K for the base scenario. As shown in (10), the sensitivity is proportional to the dot product of the gradients of the head (Figure 3a) and the adjoint function φ (Figure 5). There are two important observations that can be made on the computed sensitivity values in Figure 6. First, very close to the tool between the injection screen and the first transducer, and above the far transducer, the sensitivity is negative indicating that the DPP K estimate will increase when the K decreases in these areas, and vice versa. For most of the area in the vicinity of the tool, the DPP K estimate and aquifer K is positively related. Second, the DPP is most sensitive to the small area surrounding the interval between the injection screen and the transducers. In other words, K features located further than a few tens of centimeters below the screen or above the far transducer have a minimal impact on the DPP estimate. Horizontally, the DPP becomes largely insensitive to K features located more than ~0.5 m from the tool. Note that the sensitivity results do not change with injection rate due to the use of the steady-shape analysis. The extremely compact domain of high sensitivity enables the DPP to be an effective tool for obtaining detailed K information with minimal interference from the area outside the sampling volume.

[28] The sensitivity results shown in Figure 6 provide an explanation for the K estimates obtained in some of the single injection test scenarios. First, a skin surrounding the tool occupies both positive and negative sensitivity regions, so the net impact is dependent on both, which in turn are a function of the thickness and the K of the skin. The negative sensitivity region has slightly greater influence on the skin configurations during the initial change of skin K and thickness in Figures 4(a) and 4(b). As a result, the DPP K estimates are slightly larger than the input reference value despite the presence of the low-K skin. As the skin K decreases or the skin thickness increases further, the positive sensitivity region starts to dominate and the resulting DPP K estimates become smaller than the reference value. Second, in the clogging scenario, the DPP K estimate is larger than the reference value after incorporation of the thin low-K zone around the screen. However, because the volume of this clogged zone is extremely small, the increase in the DPP K estimate is minimal.

[29] An important advantage of the DPP is that the head field needs only be at steady-shape conditions. Figure 7 shows the head changes from the transient simulation of the base scenario for a specific storage of 5.0×10^{-6}/m. The individual head changes at the transducers have not reached steady state after 200 s. However, the difference in the head changes between the transducers stabilizes in less than a second. Although more time is obviously required in practice because injection rates do not stabilize instantaneously, the requirement that only steady-shape conditions be attained enables a tremendous reduction in the time required for a DPP test.

4.2. Single Injection Test in a Homogeneous Aquifer With a Thin Embedded Layer

[30] In this case we investigate DPP performance when a thin low- or high-K layer is embedded in an otherwise homogeneous aquifer. A particular objective is to identify how a typical DPP injection test responds to a thin anomalous layer in the vicinity of the tool. Other than the

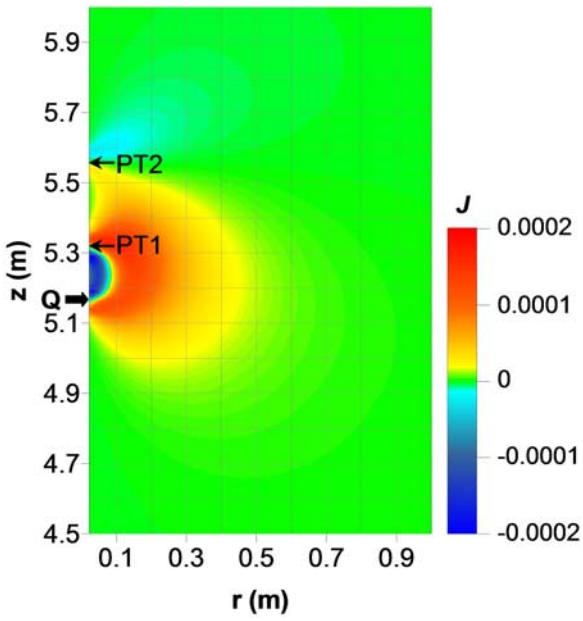

Figure 6. The sensitivity of the difference in head changes between the pressure transducers to K for the base scenario.

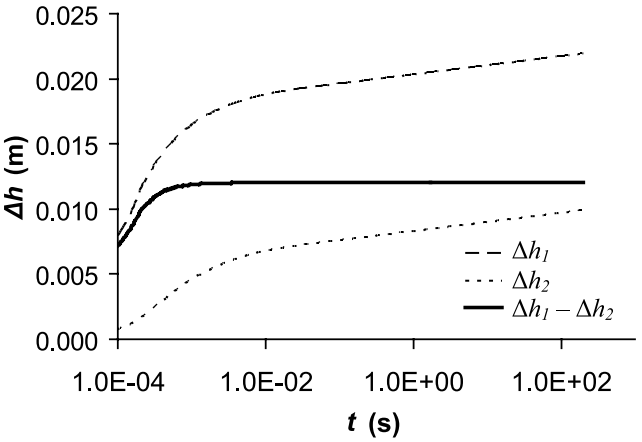

Figure 7. Comparison of time required for obtaining steady-shape versus steady state flow in a DPP test. The head changes at the individual transducers (Δh_1 and Δh_2) do not reach steady state at the end of simulation (200 s), whereas the difference in the head changes ($\Delta h_1 - \Delta h_2$) becomes constant in less than 0.1 s.

embedded layer, the K field is homogenous and isotropic (1.5×10^{-3} m/s). The embedded layer is 0.1 m in thickness with a K of either 1.5×10^{-5} m/s (a low-K barrier, such as a silty sand) or 1.5×10^{-1} m/s (a high-K channel, such as a gravel). The layer extends horizontally to the edge of the model domain.

[31] Figure 8 shows the position of the thin layer relative to the injection screen and the near and far transducers. In scenarios 1 through 7, the layer is placed, in turn, below the screen, over an interval encompassing the screen, between the screen and PT1, over an interval encompassing PT1, between PT1 and PT2, over an interval encompassing PT2, and above PT2. In each scenario, only a single anomalous layer is included and the base conditions are present elsewhere. Furthermore, as each configuration is assigned two K values, letter "a" is used to represent a low-K layer and "b" to represent a high-K layer. For example, scenario "1a" indicates that a 0.1 m-thick low-K layer is below the injection screen, while scenario "4b" indicates that a 0.1 m-thick high-K layer encompasses PT1. The induced head changes for scenarios 5a and 5b are plotted on Figures 3(d) and 3(e), respectively. Because the low-K layer impedes flow, the resulting difference in head between the transducers is greater than twice the base case. When the embedded layer is high K, the head difference is slightly below the base case due to the flow converging into that layer.

[32] Table 2 shows the DPP K estimates for scenarios 1a through 7b. The K field is taken as homogenous in the numerical inversion assuming that the existence of the embedded layer is not recognized during the parameter estimation process. The values shown for each scenario are estimated by *lr2dinv*, equation (1) using $\Delta h_1 - \Delta h_2$, equation (2) using Δh_1, and equation (2) using Δh_2. The differences between the numerical estimates from *lr2dinv* and the values computed by (1) are relatively small in all scenarios, consistent with the results of Section 4.1. When applying equation (2), K estimates based on the head change at the near transducer, PT1, are closer to those obtained from *lr2dinv* than are K estimates based on the head change at PT2.

[33] Two observations can be made based on the *lr2dinv* results in Table 2. First, the K estimate inverted from the DPP is most sensitive to conditions in the interval between the screen and PT1. Second, the DPP K estimate is not a simple geometric or any other mean of the aquifer K and the K of the embedded layer. Instead, the DPP K estimate is dependent on both the position and the K value of the layer. In some scenarios (e.g., 2b, 3a, 3b, and 4b), the DPP K estimates are heavily affected by the embedded layer, clearly demonstrating the insufficiency of a single test for determining the K of thin layers. As shown in the following sections, a joint inversion of multiple DPP tests is necessary for quantifying such small-scale K variations.

[34] The sensitivity results in Figure 6 provide some explanation for the K estimates obtained in Table 2. First, the sensitivity is negative above the far transducer PT2. When a low-K layer is placed above PT2 (scenario 7a), the DPP K estimate determined from *lr2dinv* or equation (1) is larger than the reference value. Similarly, the K estimate is smaller than the reference value when the inclusion is a high-K layer (scenario 7b). Second, the sensitivity is positive between transducers PT2 and PT1 and below the injection screen. The DPP K estimate is smaller than the reference value when a low-K layer is included in these areas (scenarios 5a and 1a), and is larger when there is a high-K layer (scenarios 5b and 1b). Third, the sensitivity contains both negative and positive values between PT1 and the injection screen. The impact of an anomalous K layer in this interval is complicated, as the DPP K estimate depends on the thickness and value of the layer.

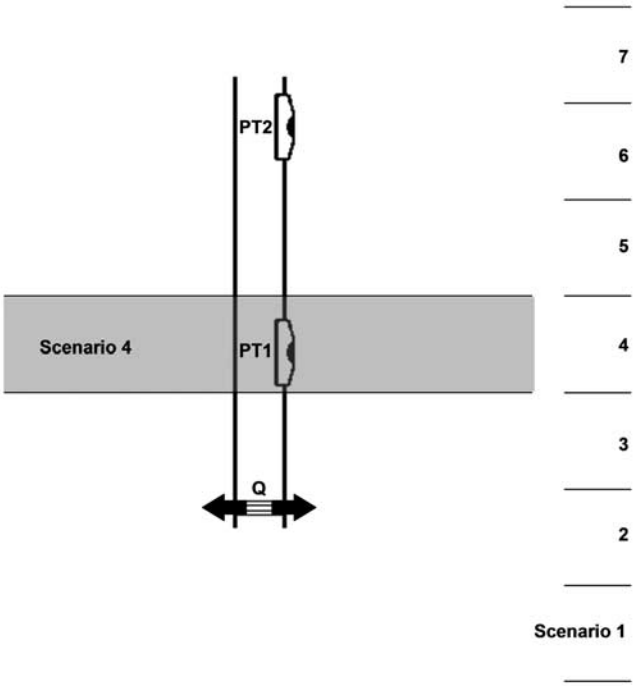

Figure 8. The position of the thin low- or high-K layer relative to the DPP injection screen and pressure transducers for the different scenarios in section 4.2. The left part of the diagram shows the example of scenario 4 in which the thin layer is represented as the shaded interval encompassing PT1 in an otherwise homogenous aquifer. Scenario numbers are shown on the right.

Table 2. The DPP K Estimates for Scenarios When a Thin Low- or High-K Layer is Embedded in an Otherwise Homogeneous Aquifer[a]

		Scenario Letter							
		a (Low K)				b (High K)			
		lr2dinv	equation (1)	equation (2) K_1	equation (2) K_2	*lr2dinv*	equation (1)	equation (2) K_1	equation (2) K_2
Scenario Number	7	1.81	1.99	1.62	1.23	1.28	1.42	2.04	7.55
	6 (PT2)	1.03	1.25	1.51	2.28	1.32	1.46	2.25	22.52
	5	0.54	0.83	1.30	21.11	1.76	1.94	2.93	20.73
	4 (PT1)	0.52	0.63	1.00	21.13	37.27	44.25	31.07	20.77
	3	22.24	26.51	24.19	21.1	22.25	26.19	23.82	20.71
	2 (Screen)	0.97	1.07	1.21	1.55	28.6	34.48	29.43	23.66
	1	1.07	1.18	1.22	1.31	2.53	2.79	3.43	5.58

[a]The values shown for each scenario are estimated by *lr2dinv*, equation (1) using $\Delta h_1 - \Delta h_2$, equation (2) using Δh_1, and equation (2) using Δh_2, respectively. Scenario number indicates the relative position of the thin layer (Figure 8)], and scenario letters "a" and "b" stand for a low- and high-K layer, respectively. K is in 10^{-3} m/s.

[35] When an anomalous layer occurs in the vicinity of the DPP, additional data and analyses are necessary for identifying its position and properties accurately. As mentioned in Section 2, the use of equation (2) with the individual steady state head changes at PT1 and PT2 can provide some insight into the location of the layer in certain circumstances. Table 2 shows the K values computed using (2) with the head changes at PT1 and PT2 (i.e., K_1 and K_2), respectively, for scenarios 1a through 7b. The most striking differences between K_1 and K_2 occur when 1) the low-K layer encompasses PT1 (scenario 4a) or is between PT1 and PT2 (scenario 5a), or 2) the high-K layer is located between PT1 and PT2 (scenario 5b) or encompasses PT2 (scenario 6b). It is interesting to note that in these scenarios, K_2 is always larger than K_1, regardless of the specific low- or high-K value assigned to the embedded layer. Therefore a simple calculation using equation (2) can serve as a qualitative indicator of an anomalous high- or low-K layer between PT1 and PT2. To determine the specific K of that layer, however, more data and analyses are needed. In the following sections, we investigate whether simultaneous analysis of multiple injection tests at different depths can be used to quantify spatial variations in K more accurately.

4.3. Multiple Injection Tests in a Heterogeneous Aquifer

[36] To characterize vertical K variations in a heterogeneous setting, multiple DPP injection tests need to be conducted at different depths. The 12 K zones measured at the GEMS research site (Figure 2) are used as the input K during the forward simulations. Five different scenarios are considered here. In scenario I, the same K zonation as in the forward simulations is used in the inverse analysis, assuming that prior information on the K structure is available. In the field such information can be obtained by monitoring the injection rate and pressure during DPP advancement [*Dietrich et al.*, 2008]. A total of 18 injection tests are simulated with the first injection interval 9.150 to 9.175 m above the bottom of aquifer, followed by a sequence of tests at 0.5-m intervals. The last injection interval is 0.650 to 0.675 m above the base of the aquifer. The head changes from all tests are analyzed simultaneously for inverting the K values. Figure 9 shows the joint K estimates from *lr2dinv* at different depths in scenario I along with the 12 reference values. The numerical DPP K estimates are in very close agreement with the reference values when the K zonation is assumed known during the inverse estimation process.

[37] Figure 10 displays the calculated sensitivity for the 18 injection tests of scenario I. Results are for the root mean square of sensitivity over all 18 injection tests,

$$RMS_i = \sqrt{\sum_{k=1}^{18} \left(J_i^k\right)^2 / 18}, \tag{11}$$

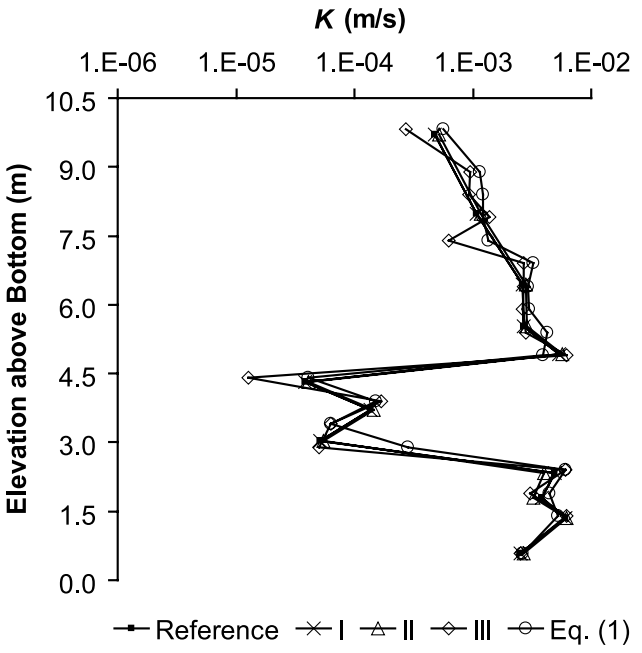

Figure 9. DPP K estimates for different scenarios in Section 4.3 when multiple injection tests are conducted in a heterogeneous K field. Also shown for comparison are the reference 12 zone K values from the GEMS research site and the 18 K values calculated from the individual tests with the analytical formula (1). The K estimates of scenario I are essentially the same as the reference values. In scenario II a low-K skin is included. In scenario III the reference K zonation is assumed unknown during the parameter estimation process.

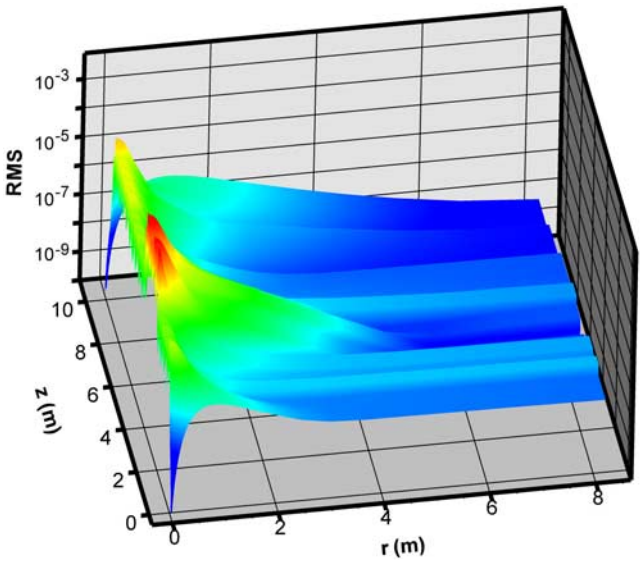

Figure 10. The sensitivity of the difference in the head changes between the two transducers to K for the 18 injection tests. The 12 reference K values in scenario I in section 4.3 are used as the base K. Results are the root mean square of the sensitivity values over all 18 injection tests.

where J_i^k is the sensitivity of the head change to the K value in grid cell i for the k-*th* injection test. Figure 10 indicates that the distribution of high sensitivity zones is consistent with the position of each injection test. Conceivably, when the depth interval of successive DPP advancement is sufficiently small, the high sensitivity domains would form a continuous vertical column surrounding the DPP borehole. Furthermore, the sensitivity results are strongly dependent on the base K values. There are several low-K layers between elevations 2.5 and 4.5 m. Correspondingly, the sensitivity values computed within this interval are much larger than those at other depths. Horizontally, the sensitivity values become relatively small when the distance is greater than ~0.5 m away from the DPP.

[38] In scenario II, we include a low-K skin ($K = 1.0 \times 10^{-5}$ m/s, thickness 0.02 m) in the forward simulation. For simplicity, the skin is extended through the entire aquifer thickness. Again, the low-K skin is not explicitly specified during numerical inversion, assuming that no information on the skin is available. All other settings remain identical to those in scenario I. Figure 9 displays the DPP K estimates after incorporating the low-K skin in the forward simulation. The differences between the DPP estimates and the reference K values are insignificant, indicating that this low-K skin does not have a large impact on DPP K estimates in a heterogeneous field.

[39] In many cases, prior information on the K structure may not be available. In scenario III, we investigate how the DPP performs under such conditions by disregarding the reference K zonation in the inverse analysis. Instead of using the reference zonation, a total of 18 K zones are defined during the parameter estimation process. Each zone corresponds to the injection test at a certain depth and is bounded by the zones for the two adjacent tests. As a result, the thickness of most zones is 0.5 m, except for the top and bottom zones, which are bounded, respectively, by the upper and lower boundaries of the aquifer. The top zone is 1.15 m thick and the bottom zone is 1.10 m thick. All other settings are identical to those in scenario I. The DPP K estimates in scenario III are presented in Figure 9. Despite the local mismatch at some depths due to the different zonations, the K estimates from the DPP are in good agreement with the reference values overall. While prior knowledge of the K structure is essential for estimating the K values to a high degree of accuracy, the DPP can be used, with some degradation in accuracy, to determine both the structure and magnitude of K.

[40] To assess the applicability of the steady-shape analytical formula in heterogeneous settings, equation (1) is applied to each of the 18 tests in scenario III. Figure 9 displays the 18 analytical K estimates. Similar to the numerical *lr2dinv* estimates, the analytical results are in good agreement with the reference values overall, suggesting that equation (1) can be applied to heterogeneous settings when the distance over which K is varying is larger than that between the screen and the far transducer.

[41] In scenario IV, we investigate the ability of the DPP to quantify K features that are thin relative to the DPP tool dimensions. Previous simulations in Sections 4.1 and 4.2 have shown that a single DPP injection test provides an effective K for the area immediately surrounding the 0.4-m interval between the injection screen and the far transducer. Simultaneous analysis of multiple injection tests at different vertical positions allows the DPP to quantify K features that are thinner than 0.4 m, given that the vertical interval between successive DPP tests is sufficiently small. To demonstrate the fine resolution the DPP can achieve, a 0.1 m-thick high- or low-K layer is added to the K profile from GEMS (Figure 11). The K value is set to 5.0×10^{-2} m/s and 5.0×10^{-6} m/s for the added high- and low-K layers, respectively. Three different cases, referred to as A, B and C below, are investigated with this configuration.

[42] In case A, the model settings are identical to those of scenario I in Figure 9 except that the extra layer is added to the forward simulation. As a result, 13 reference K zones are involved in the forward simulations. In the inverse parameter estimation, the reference 13-zone structure (including the new thin layer) is assumed known and specified explicitly. A total of 18 tests at 0.5-m intervals are conducted at the same depths as those in scenario I. Figure 11(a) shows the results when the extra layer is specified as a high-K preferential flow channel. The DPP K estimates from case A are essentially the same as the reference values at all depths. Figure 11(b) shows the results when the extra layer is specified as a low-K flow barrier. In this case, the DPP K estimate from case A does not match with the K value for the thin layer. Instead of the input value of 5.0×10^{-6} m/s, the DPP K estimate is 1.4×10^{-2} m/s.

[43] In case B, the vertical interval between successive DPP tests is reduced from 0.5 to 0.1 m between 6.150 and 6.775 m, resulting in a total of 23 tests across the aquifer. All other settings remain identical to those in case A. During the numerical parameter estimation, the K structure is assumed known and specified explicitly. Figure 11(a) indicates that, as the true K distribution (including the high-K channel) has already been identified when 18 tests are used, the addition of more tests does not yield any change in

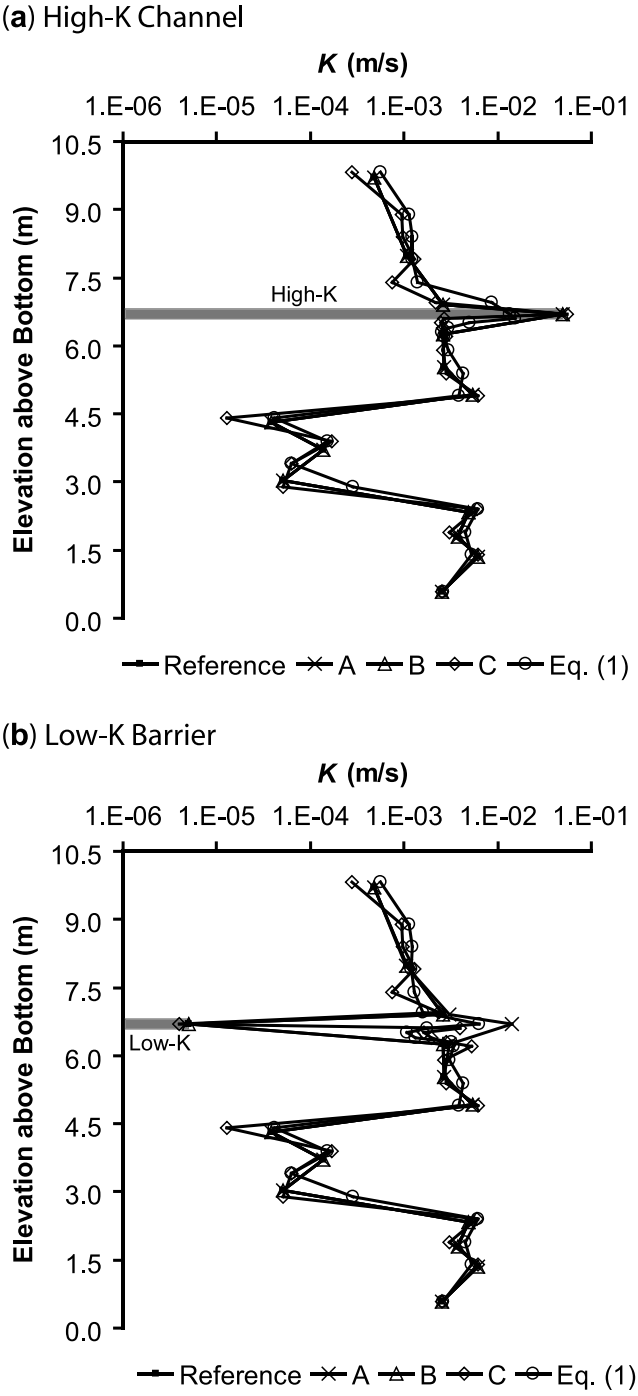

Figure 11. DPP K estimates after adding a 0.1 m-thick (a) high-K channel and (b) low-K barrier to the GEMS K profile. The extra layer is placed at elevations 6.65–6.75 m. The added low-K layer in Figure 11(b) is poorly estimated in case A. By adding a few closely-spaced injection tests below the layer, the low-K barrier is characterized much more accurately in cases B and C.

the DPP estimates. Figure 11(b), on the other hand, shows that the accuracy of the DPP K estimates is improved dramatically after five additional tests are conducted in the interval immediately below the thin low-K layer. It should be emphasized that such an adjustment to the vertical interval between tests is practically feasible under field conditions, as qualitative K information can be obtained by monitoring the injection pressure continuously during DPP advancement [*Dietrich et al.*, 2008]. Therefore whenever there is a significant reduction in K as indicated by a sharp increase in injection pressure, the advancement interval can be reduced to characterize that low-K feature.

[44] Case C is similar to B except that the reference K zonation is assumed unknown during the parameter estimation process. A total of 23 K zones are used in the inverse simulation. Each zone is specified in accordance with the injection test at a certain depth. Figure 11(a) shows that, despite the local mismatch produced by the different zonations for the forward and inverse simulations, the DPP K estimates are in good agreement with the reference K values, including at the thin high-K channel. Figure 11(b), however, shows that without using the reference K zonation, the accuracy of the DPP K estimates decreases, particularly in the area immediately below the thin low-K layer where spurious oscillation in the K estimates is observed. Thus prior knowledge of the K structure is more critical in the case of a thin low-K layer.

[45] To demonstrate the importance of simultaneous analysis of DPP tests in the presence of small-scale K variations, the analytical formula (1) is applied to each of the 23 tests in case C. Figure 11 indicates that the analytical K estimates do not match the reference K values for either the high-K channel or the low-K barrier. While equation (1) is still effective for quantifying K variations at a scale greater than the interval between the injection screen and the far transducer (>0.4 m), simultaneous analysis of all DPP tests is necessary for accurately obtaining the K information at smaller scales (<0.4 m).

[46] In scenario V, we explore how the DPP responds to lateral variations in K by adding a low- or high-K zone, which has an inner boundary at a radial distance from the DPP, to the test configuration of scenario III. Results show that when that inner boundary is at lateral distances greater than 0.51 m from the DPP, the K estimates are essentially the same as those in the reference case (i.e., the DPP K estimates are unaffected by that zone, consistent with the sensitivity results in Figures 6 and 10). Because of the assumed symmetry in the angular direction, the added zone is in the form of a hollow cylinder with an outer boundary that extends to the edge of the model domain. For a planar or block feature, the influence on the K estimates would be smaller for the same distance from the DPP to the inner boundary of the zone.

5. Summary and Conclusions

[47] As it becomes increasingly evident that variations in hydraulic conductivity (K) over very short distances can exert a significant influence on subsurface transport processes [*Boggs et al.*, 1993; *Feehley et al.*, 2000; *Harvey and Gorelick*, 2000; *Liu et al.*, 2004; *Berkowitz et al.*, 2006], there is a critical need to develop effective tools for accurate description of such variations in the field. On the basis of work at two controlled field sites, *Butler et al.* [2007] have shown that the direct-push permeameter (DPP) offers a promising means of characterizing vertical variations in K at an unprecedented level of detail, accuracy and speed. In

this paper the fundamental efficacy of the DPP is evaluated rigorously through a series of numerical simulations based on results from field work performed at the Geohydrologic Experimental and Monitoring Site [*Butler*, 2005; *Butler et al.*, 2007; *Bohling et al.*, 2007]. These simulations demonstrated that the DPP should provide an accurate, high-resolution K profile in many situations commonly faced in the field.

[48] The primary findings of this simulation investigation are as follows. First, the simple analytical formula (1) provides reasonable K estimates when homogeneous conditions can be assumed in the vicinity of the tool. However, due to the deviation from the ideal assumptions of point injection and spherical flow in an infinite homogeneous field, numerical analysis is needed to determine K more accurately under general field conditions. Second, equation (2) can provide a qualitative indicator of the potential existence of thin layers of relatively high or low K between the two pressure transducers. Third, a typical low-K skin created by material compaction during tool advancement (i.e., skin K within one order of magnitude of the aquifer K) only has a small impact on the accuracy of the DPP K estimates. Fourth, when the aquifer is anisotropic, the DPP gives an estimate close to the horizontal component K_r. Fifth, the requirement that only steady-shape flow conditions be attained during a DPP injection test allows for a dramatic reduction in the time required for each test. Thus the tool can be a very efficient means of characterizing vertical variations in K in the field. Sixth, a single DPP test is most sensitive to the area immediately surrounding the interval between the injection screen and the most distant transducer. Horizontally, the DPP shows little sensitivity to K features greater than $\sim$0.5 m away from the tool. As a result, the DPP is able to provide high-resolution profiles of vertical K variations with minimum influence from lateral variations outside its immediate vicinity. Seventh, the DPP resolution can be increased significantly by advancing at smaller vertical intervals in the area of interest. Simultaneous analysis of all DPP tests is necessary for accurately describing the K variations at a scale smaller than the interval between the screen and the far transducer (i.e., $<$0.4 m). Eighth, prior information on the K structure helps increase the accuracy of K estimates, especially in the presence of thin low-K layers that serve as barriers to flow. Such information can be obtained in the field by monitoring the injection pressure continuously during tool advancement.

[49] In this numerical investigation, the DPP has been evaluated in confined flow conditions. Except in the immediate vicinity of the water table, the findings presented here will also be applicable to unconfined systems. The water table should be explicitly included in the model used in the inverse estimation procedure for DPP tests performed near the top of an unconfined aquifer.

[50] This work shows that the DPP can be used to accurately characterize K variations along a vertical profile. The narrowly focused sensitivity of the DPP must be considered one of the primary strengths of this technique. However, a defensible characterization of the lateral continuity of layers cannot be obtained from one or a series of DPP profiles. Future work is needed to explore the utility of the DPP, possibly in conjunction with geophysical methods, to delineate the lateral continuity of layering. Moreover, the configuration shown in Figure 1 is just one of many possible DPP designs. In order to get the most information from this technique, further research is needed to investigate other possible configurations of this promising characterization tool.

[51] **Acknowledgments.** The authors are grateful to Olaf Cirpka, Keith Halford and two anonymous reviewer for constructive comments that led to the improvement of this paper.

References

Berkowitz, B., A. Cortis, M. Dentz, and H. Scher (2006), Modeling non-Fickian transport in geological formations as a continuous time random walk, *Rev. Geophys.*, *44*, RG2003, doi:10.1029/2005RG000178.

Boggs, J. M., L. M. Beard, S. E. Long, M. P. McGee, W. G. MacIntyre, C. P. Antworth, and T. B. Stauffer (1993), Database for the Second Macrodispersion Experiment (MADE-2), *Tech. Rep. TR-102072*, Electric Power Res. Inst., Palo Alto, California.

Bohling, G. C., and J. J. Butler Jr. (2001), Lr2dinv: A finite-difference model for inverse analysis of two-dimensional linear or radial groundwater flow, *Comput. Geosci.*, *27*(10), 1147–1156.

Bohling, G. C., X. Zhan, J. J. Butler Jr., and L. Zheng (2002), Steady-shape analysis of tomographic pumping tests for characterization of aquifer heterogeneities, *Water Resour. Res.*, *38*(12), 1324, doi:10.1029/2001WR001176.

Bohling, G. C., J. J. Butler Jr., X. Zhan, and M. D. Knoll (2007), A Field Assessment of the Value of Steady-shape Hydraulic Tomography for Characterization of Aquifer Heterogeneities, *Water Resour. Res.*, *43*, W05430, doi:10.1029/2006WR004932.

Butler, J. J., Jr. (1990), The role of pumping tests in site characterization: Some theoretical considerations, *Ground Water*, *28*(3), 394–402.

Butler, J. J., Jr. (2005), Hydrogeological methods for estimation of hydraulic conductivity, In *Hydrogeophysics*, edited by Y. Rubin and S. Hubbard, Springer, The Netherlands, pp. 23–58.

Butler, J. J., Jr., and C. D. McElwee (1995), *Well-testing methodologies for characterizing heterogeneities in alluvial-aquifer systems: final technical report*, Kansas Geological Survey Open File Report 95-75.

Butler, J. J., Jr., J. M. Healey, G. W. McCall, E. J. Garnett, and S. P. Loheide II (2002), Hydraulic tests with direct-push equipment, *Ground Water*, *40*(1), 25–36.

Butler, J. J., Jr., P. Dietrich, V. Wittig, and T. Christy (2007), Characterizing hydraulic conductivity with the direct-push permeameter, *Ground Water*, *45*(4), 409–419.

Dietrich, P., and C. Leven (2005), Direct Push Technologies, In *Groundwater Geophysics*, edited by R. Kirsch, Springer, 321–340.

Dietrich, P., J. J. Butler, and K. Faiß (2008), A rapid method for hydraulic profiling in unconsolidated formations, *Ground Water*, in press.

Feehley, C. E., C. Zheng, and F. J. Molz (2000), A dual-domain mass transfer approach for modeling solute transport in heterogeneous porous media, application to the MADE site, *Water Resour. Res.*, *36*(9), 2051–2515.

Harvey, C. F., and S. M. Gorelick (2000), Rate-limited mass transfer or macrodispersion: Which dominates plume evolution at the Macrodispersion Experiment (MADE) site?, *Water Resour. Res.*, *36*(3), 637–650.

Hinsby, K., P. L. Bjerg, L. J. Andersen, B. Skov, and E. V. Clausen (1992), A mini slug test method for determination of a local hydraulic conductivity of an unconfined sandy aquifer, *J. Hydrol.*, *136*(1–4), 87–106.

Liu, G., C. Zheng, and S. M. Gorelick (2004), Limits of applicability of the advection-dispersion model in aquifers containing connected high-conductivity channels, *Water Resour. Res.*, *40*, W08308, doi:10.1029/2003WR002735.

Lowry, W., N. Mason, V. Chipman, K. Kisiel, and J. Stockton (1999), *In-situ permeability measurements with direct push techniques: Phase II topical report*, SEASF-TR-98-207 Rept. to DOE Federal Energy Tech. Center, 102 pp.

Lunne, T., P. K. Robertson, and J. J. M. Powell (1997), *Cone Penetration Testing in Geotechnical Practice*, London: Blackie Academic and Professional.

McCall, W., J. J. Butler Jr., J. M. Healey, A. A. Lanier, S. M. Sellwood, and E. J. Garnett (2002), A dual-tube direct-push method for vertical profiling of hydraulic conductivity in unconsolidated formations, *Environ. Eng. Geosci.*, *8*(2), 75–84.

McCall, W., D. M. Nielsen, S. Farrington, and T. C. Christy (2005), Use of direct-push technologies in environmental site characterization and ground-water monitoring, In *The Practical Handbook of Environmental*

Site Characterization and Ground-Water Monitoring (2nd Edition), edited by D. M. Nielsen, CRC, 345–472.

Press, W., S. Teukolsky, W. Vetterling, and B. Flannery (1992), *Numerical Recipes in C* (2nd Edition), Cambridge Univ. Press, Cambridge.

Schulmeister, M. K., J. J. Butler Jr., J. M. Healey, L. Zheng, D. A. Wysocki, and G. W. McCall (2003), Direct-push electrical conductivity logging for high-resolution hydros-tratigraphic characterization, *Ground Water Monit. Rem.*, *23*(3), 52–62.

Sellwood, S. M., J. M. Healey, S. Birk, and J. J. Butler Jr. (2005), Direct-push hydrostratigraphic profiling: Coupling electrical logging and slug tests, *Ground Water*, *43*(1), 19–29.

Stienstra, P., and J. K. van Deen (1994), Field data collection techniques – unconventional sounding and sampling methods, In *Engineering Geology of Quaternary Sediments*, ed. by N. Rengers, 41–55.

Sun, N. Z. (1994), *Inverse Problems in Groundwater Modeling*, Kluwer Acad., Norwell, Mass.

Sykes, J. F., J. L. Wilson, and R. W. Andrews (1985), Sensitivity analysis for steady state groundwater flow using adjoint operators, *Water Resour. Res.*, *21*(3), 359–371.

G. C. Bohling, J. J. Butler Jr., and G. Liu, Kansas Geological Survey, University of Kansas, Lawrence, KS, USA. (gliu@kgs.ku.edu)